NANO LETTERS

pubs.acs.org/NanoLett

Letter

High-Speed AFM Reveals Molecular Dynamics of Human Influenza A Hemagglutinin and Its Interaction with Exosomes

Keesiang Lim, Noriyuki Kodera, Hanbo Wang, Mahmoud Shaaban Mohamed, Masaharu Hazawa, Akiko Kobayashi, Takeshi Yoshida, Rikinari Hanayama, Seiji Yano, Toshio Ando, and Richard W. Wong*

Cite This: *Nano Lett.* 2020, 20, 6320−6328

Read Online

ACCESS | Metrics & More | Article Recommendations | Supporting Information

ABSTRACT: Influenza A hemagglutinin (HA) is one of the crucial virulence factors that mediate host tropism and viral infectivity. Presently, the mechanism of the fusogenic transition of HA remains elusive. Here, we used high-speed atomic force microscopy (HS-AFM) to decipher the molecular dynamics of HA and its interaction with exosomes. Our data reveal that the native conformation of HA in the neutral buffer is ellipsoidal, and HA undergoes a conformational change in an acidic buffer. Real-time visualization of the fusogenic transition by HS-AFM suggests that the mechanism is possibly fit to the "uncaging" model, and HA intermediate appears as Y-shaped. A firm interaction between the HA and exosome in an acidic buffer indicates the insertion of a fusion peptide into the exosomal layer and subsequently destabilizes the layer, resulting in the deformation or rupture of exosomes, releasing exosomal contents. In contrast, the HA−exosome interaction is weak in a neutral buffer because the interaction is mediated by weak bonds between the HA receptor-binding site and receptors on the exosome.

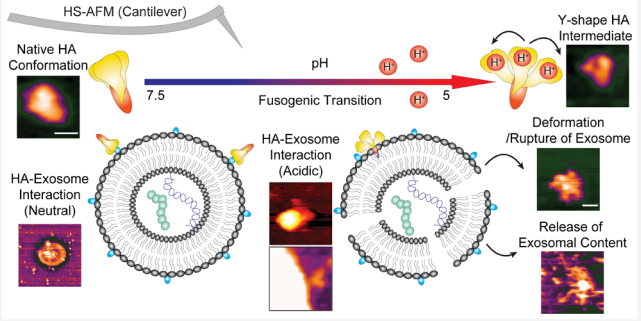

KEYWORDS: *high-speed atomic force microscopy, influenza A, hemagglutinin, exosomes, fusogenic transition*

Flu is a major public health problem that has imposed a great socioeconomic burden on many countries. Flu viruses are the members of the family *Orthomyxoviridae*. The genus *Influenzavirus A* (IAV) is the most devastating flu virus to human beings. According to the WHO, the estimated annual influenza infection is approximately 1 billion cases[1] and 300 000−500 000 deaths.[2] Influenza A hemagglutinin (HA) is one of the most crucial virulence factors of IAV. The properties of HA determine host tropism, infectivity, transmissibility, and the risk of a human pandemic. HA plays a pivotal role in orchestrating the entry of IAV into host cells to release a viral ribonucleoprotein. HA is synthesized as a trimeric precursor known as HA0, and later, it will be cleaved by host proteases to become fusion compatible. There are a total of 18 different subtypes of HA (H1−H18), and their protein structures are relatively similar.[1] HA consists of two main subunits: HA1 and HA2. The globular head domain in HA1 has a receptor-binding site (RBS) that allows HA binding to its receptor, the sialic acid-linked galactose, expressed on the host cell membrane.[3] The HA2 subunit contains a coiled-coil stalk domain and transmembrane subdomain for stabilization of the HA trimer and for anchoring HA in a viral membrane.[3] The fusion peptide at the N terminus of the HA2 subunit is required for membrane fusion.[4] After HA binds to its receptor, the virus enters into the host cell via endocytosis. In a neutral environment, HA is metastable, and it is easily triggered by the acidic endosomal environment to undergo a conformational change to release a fusion peptide. This process is known as fusogenic transition. Insertion of a fusion peptide into the endosomal membrane is needed to mediate the fusion of a viral membrane and endosomal membrane.[5−7]

The nanostructural properties of HA have been extensively studied for decades. Molecular dynamics of HA at a fusogenic pH is the major concern for developing neutralizing antibodies, as most of these antibodies target the epitopes in the RBS (for blocking viral attachment and membrane fusion) or the epitopes in the stalk domain (for blocking membrane fusion).[8] X-ray crystallography is a powerful tool for structural analysis of proteins because this technique yields high atomic resolution data that allows scientists to identify important functional sites in target proteins. Although a prefusion HA structure has been characterized by this technique,[9] owing to

Received: April 22, 2020
Revised: July 25, 2020
Published: July 27, 2020

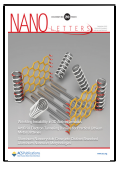

https://dx.doi.org/10.1021/acs.nanolett.0c01755
Nano Lett. 2020, 20, 6320−6328

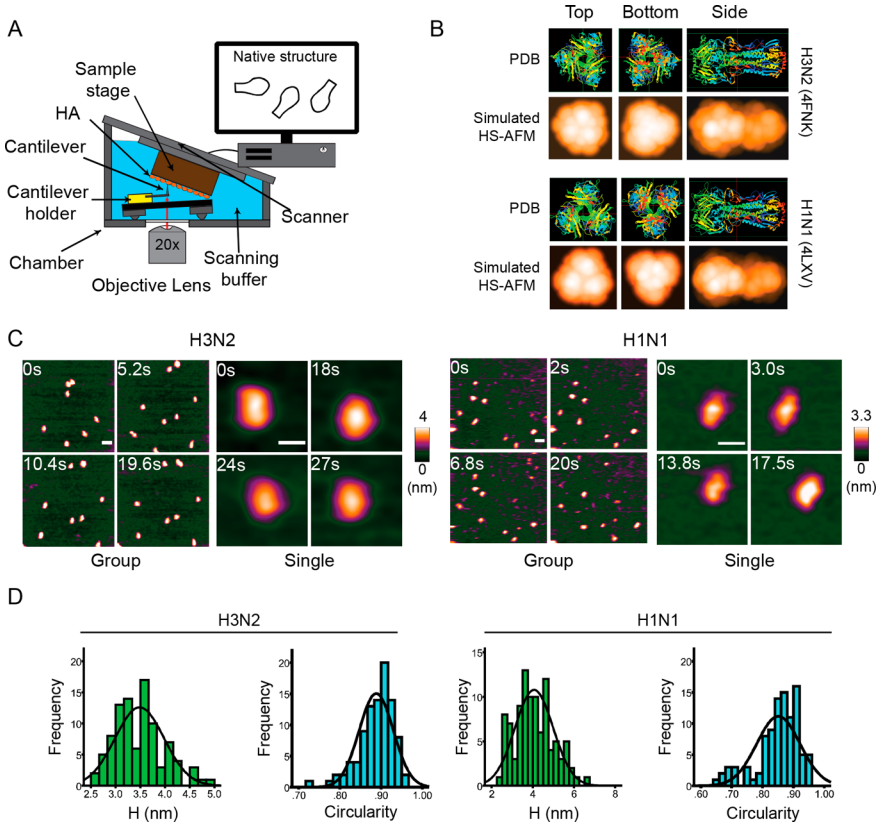

Figure 1. Direct real-time visualization of the native conformation of HA using HS-AFM. (A) Schematic diagram illustrating the setup of HS-AFM for scanning HA in physiological buffers. (B) Generation of simulated HS-AFM images of HA using publicly available PDB data (PDB code for H3 HA (H3N2), 4FNK; PDB code for H1 HA (H1N1), 4LXV). (C) HS-AFM scanning of HA proteins in 50 mM Tris HCl at pH 7.6. Briefly, HA proteins were loaded on a bare mica surface, and then the proteins were scanned using HS-AFM. Results are depicted either in a group of molecules or in a single molecule (scale bar: group$_{H3}$, 40 nm; group$_{H1}$, 30 nm; single, 15 nm). (D) Spatial analysis of HA proteins in a neutral condition. The results are presented in histograms with normal distribution curves (n_{H3}, 94; n_{H1}, 101; *H*, height).

its intrinsic technical limitations (for example, issues of protein crystallization and static images) and the transient nature of HA intermediates, X-ray crystallography is not an ideal approach for characterizing the intermediate and postfusion structures of HA.[10] Characterization of the postfusion conformation of HA using X-ray crystallography is insufficient as the findings so far, only covering fragmentary information on the HA2 subunit[9,11] and details of the monomeric HA1 subunit−antibody complex.[12] Different approaches such as spectroscopy,[13−16] limited proteolysis,[17−20] epitope exposure mapping,[18,20] cryo-EM,[21,22] and smFRET[23] have been used by researchers to reinforce the existence of intermediate forms of HA in acidic environments. The fusogenic transition of HA involves dissociation of the trimeric globular head domain of HA1 and a loop-to-helix conformational change of HA2 to translocate the fusion peptide to the target membrane. The transition was initially thought as an irreversible one-way process or more profoundly known as a "spring-loaded" conformational change;[6] yet, the existence of HA intermediates indicates that the fusogenic transition, rather than a cascading process. The initial conformational change of HA triggered by acidification remains unknown. According to Godley et al.,[24] dissociation of the trimeric globular head domain of HA1 was a prerequisite for the reorganization of HA2 to the release fusion peptide. On the contrary, Kemble et al. reported that partial dissociation of the trimeric globular head domain of HA1 exposed HA2 in an acidic environment, in which the fusion peptide may release to contact the target membrane before complete dissociation of the globular head domain of HA1.[25] Due to a lack of direct visualization of this process, the exact mechanism of the fusogenic transition of HA is still inconclusive. Currently, two different models, the "fusion peptide release" (FP release) model[9,18,20,21,26,27] and the "uncaging" model,[3,28,29] are available to explain this biological phenomenon. The "uncaging" model proposes that the trimeric globular head domain of HA1 works as a clamp or lock to keep the fusion peptide sequestered within HA2. Protonation of HA1 dissociates the globular head domain, and this unlocks the fusion peptide by reorganizing HA2 to acquire the trimeric coiled-coil conformation (also known as the extended intermediate or prehairpin intermediate).[10] In contrast, the "fusion peptide release" model suggests that acidification of HA releases the fusion peptide, and the fusion peptide then contacts the target membrane, followed by complete dissociation of the trimeric globular head domain of HA1 and the formation of the prehairpin intermediate.[10] Once the prehairpin intermediate forms, membrane fusion can be executed, and the conformation of HA eventually changes to postfusion conformation. The order of events in the fusogenic transition of HA is the crucial knowledge gap that needs to be solved in order to fully understand the molecular dynamics of HA during membrane fusion. Furthermore, conformational dynamics of HA during its interaction with the endosomal membrane remains elusive.

The advent of high-speed atomic force microscopy (HS-AFM) has changed the field of biology considerably.[30] Unlike

https://dx.doi.org/10.1021/acs.nanolett.0c01755
Nano Lett. 2020, 20, 6320−6328

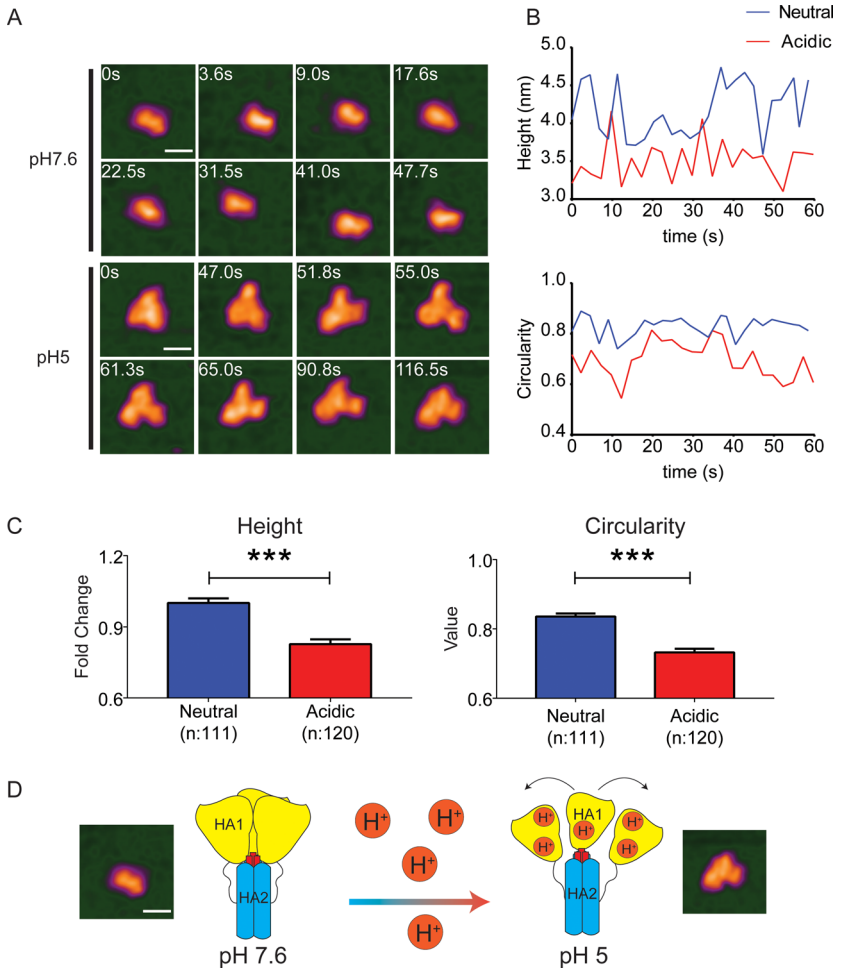

Figure 2. Acid-induced conformational change of H3 HA captured by HS-AFM. (A) H3 HA incubated either in neutral buffer or in an acidic buffer for 30 min at room temperature before HS-AFM scanning. Acidification induced structural change of H3 HA from an ellipsoid to Y-shaped (scale bar = 15 nm). (B) Real-time measurement of height and circularity of a single H3 HA after incubation either in the neutral or acidic buffer. (C) Acidification of H3 HA significantly reduced the height and circularity of H3 HA. Differences in these parameters between the two groups were calculated using the Mann−Whitney U test. Data are presented as mean ± sem (***$p < 0.001$). (D) Schematic model shows the uncaging model together with HS-AFM images of H3 HA. Protonation of the HA1 subunit of H3 HA causes dissociation of the HA1 trimer, resulting in conformational change.

conventional AFM, which has a slow scanning rate, HS-AFM can scan a biological molecule in 100 ms or less.[31] The feedback bandwidth and short cantilever in HS-AFM allow high spatiotemporal resolution scanning without affecting the integrity of biomolecules.[31] The greatest advantage of HS-AFM is the real-time imaging of biomolecules. In addition, sample preparation, for example, crystallization or fixation, is unnecessary for HS-AFM scanning to observe native or transformed conformations of target biomolecules. Therefore, this advantage overcomes the technical limitations that exist in the aforementioned techniques. By using HS-AFM, we have achieved several remarkable breakthroughs in biomolecular imaging, including structural characterization, visualization of conformational dynamics,[32] and revealing the dynamic interactions of biomolecules[33] and organelles.[34,35] Recently, we have successfully conducted a pilot study regarding real-time visualization of the native structure and conformational dynamics of the hemagglutinin precursor (HA0) of H5N1 in the physiological buffer.[36]

On the basis of these reports, we suggest that HS-AFM is a feasible tool for further investigating the native structure and molecular behavior of human IAV HA. To directly visualize the native conformation of HA, proteins were loaded on bare mica and then scanned by HS-AFM under physiological buffer (50 mM Tris HCl, pH 7.6), as shown in the schematic diagram, Figure 1A. Before we scanned the HA proteins, we first computed simulated HS-AFM images of HA (both H1 HA (H1N1) and H3 HA (H3N2)) using the PDB data downloaded from the RCSB PDB website (Figure 1B). HS-AFM images show that the native structures of HA (Figure 1C, Figures S1 and S2, Movies 1 and 2) are comparable to their corresponding crystal structures (PDB images) and simulated HS-AFM images. In a neutral buffer, multiple HA proteins did not form rosette patterns (assembly of HA proteins to a rose-like pattern) because these proteins are only HA ectodomains. The hydrophobic transmembrane domain is required for HA to form the rosette pattern in buffer.[37] The orientation of adsorption on mica depends on the surface area of HA. Our data show that most of the HA molecules appeared to be ellipsoids (side view), in which this orientation has the largest surface area. The weak tapping force in the cantilever is minimally invasive to HA, and thus, we can scan our sample for a long time without deforming HA. To overcome the tip convolution issue, we performed nanofabrication, known as

https://dx.doi.org/10.1021/acs.nanolett.0c01755
Nano Lett. 2020, 20, 6320−6328

electron-beam deposition (EBD), on the cantilever tip to produce a long and sharp tip with a small apical surface.[35] We used ImageJ to remove noises in HS-AFM images and then analyzed the images for measuring the height and circularity (Figure 1D). The circularity of HA elaborates the roundness of HA, in which a circularity value of 1.0 represents a perfect circle, and the value approaching zero indicates an increasingly elongated polygon. We compared our results with the values measured from PDB files using the JSmol, the application available on the RCSB PDB website (Table S1). Our results are close to the values measured using JSmol and values reported in previous studies either by X-ray crystallography[38] or by cryo-EM.[22] Other factors that can cause such variations are adsorption force, cantilever tapping force, protein rigidity/flexibility, and surface roughness of the substrate. The typical spatial resolution of HS-AFM is 2−3 nm in the lateral direction and approximately 0.15 nm in the vertical direction.[39] Although the spatial resolution of HS-AFM is not as high as X-ray crystallography, this technique is capable of producing reliable results for the structural analysis of proteins.

To determine the low pH-induced conformational change of HA, we first incubated H3 HA either in acidic (pH: 5) or in neutral (pH: 7.6) buffers (50 mM sodium acetate) for 30 min at room temperature follow by HS-AFM scanning. We found noticeable conformational differences in the acidic group compared with its control (Figure 2A, Figure S3A, and Movie 3). After H3 HA was exposed to acidic conditions, both height and circularity of H3 HA were significantly reduced (Figure 2B,C, and Figure S3B). These results indicate that the flexibility of H3 was increased during its conformational changes. In addition, western blot result also indicated that H3 HA underwent conformational change in acidic buffer as this change made H3 HA1 became susceptible to trypsin digestion (Figure S3C). To directly visualize the real-time fusogenic transition of H3 HA, we first loaded H3 HA on mica and scanned under neutral buffer (50 mM sodium acetate, pH 7.6). During scanning, we added acetic acid into the chamber to trigger the low pH-induced conformation change. The real-time fusogenic transition of a single H3 HA, from an ellipsoid to Y-shaped, was successfully captured (Figure S4A and Movie 4). Throughout the transition, both height and circularity of H3 HA were declining over time (Figure S4B), in which the trends are consistent with the trends in preincubation experiments. These results suggest that the process started with gradual protonation of HA1 subunits, then repulsion between HA1 subunits, and eventually dissociation of the HA1 trimeric structure. Unlike fluorescence techniques, HS-AFM reveals the inherent molecular dynamic of HA but no other molecules (for example, fluorescent tags). On the basis of this observation, we suggest that the fusogenic transition of H3 HA is likely to fit the "uncaging" model. We depict the model together with our HS-AFM images in Figure 2D. The crystal structure of bromelain-cleaved HA (BHA)[9,38] and the crystal structure of thermolysin-treated BHA ($TBHA_2$)[9] are the classical structures to represent prefusion and postfusion stages of HA. Intriguingly, we were unable to find the trimeric α-helical coiled-coil conformation ($TBHA_2$) during HS-AFM scanning. As mentioned earlier, sample preparation could be a crucial technical limitation for X-ray crystallography. BHA proteins aggregated in acidic conditions because conformational changes of BHA exposed the hydrophobic moiety of the fusion peptide. To overcome this issue, trypsin/thermolysin digestion was needed to solubilize the HA for crystallization. Under acidic conditions, the HA1 subunit was susceptible to trypsin/thermolysin digestion.[40,41] As a result, $TBHA_2$ only represented the fragment of HA. The data were unable to ensure whether the HA1 subunit is completely detached from HA after triggered by acidic conditions. Other assays including NMR spectroscopy, FRET, trypsin susceptibility assay, and epitope exposing mapping can only detect conformational changes but not visualization. Cryo-EM showed no obvious detachment of the HA1 subunit from HA.[21,22] Taken together, we suggest that the HA1 trimeric subunit undergoes complete dissociation but remains intact with HA during the fusogenic transition.

Dissociation of the HA1 subunit releases the fusion peptide, and then, the fusion peptide was inserted into the host endosomal membrane to orchestrate fusion between viral and endosomal membranes.[28] We did not observe any long conformation (coiled-coil structure) in H3 after incubation in an acidic buffer. The fusion peptide could remain sequestered in the hydrophobic pocket because the outside environment is hydrophilic. This property is beneficial for HA to release its fusion peptide only in the presence of the target lipid layer to avoid early inactivation of HA. In addition, we also did not capture any rosette forms (aggregation of H3 HA) in the acidic environment, and most of H3 HA were dispersed individually on the mica surface. As mentioned earlier, aggregation of BHA in the acidic buffer is the key limiting factor for X-ray crystallography to characterize the postfusion conformation of HA. The absence of a rosette form can be explained by two reasons. First, the concentration of HA used for HS-AFM is much lower compared with other techniques. For instance, the ng/mL range concentration of HA is sufficient for us to obtain good quality HS-AFM images. High concentrations of HA tend to cause aggregation regardless of the pH of scanning buffer, and aggregation severely affects the quality of the HS-AFM image. The concentration of HA used for electron microscope imaging was much higher than HS-AFM, usually in the mg/mL range.[42] Second, we could miss the rosette forms of HA during scanning as our HS-AFM scanning area is usually less than 1 μm × 1 μm. The Y-shape that we found is less likely to be a rosette form of HA because the size of the Y-shape is less than 20 nm, whereas the diameter of the rosette is about 37 nm.[42] Furthermore, rosettes shown in electron micrographs had more than three spikes.[42] In fact, our real-time observation of the H3 HA fusogenic transition (Figure S4) was a single-molecule observation. Therefore, the Y-shape is the transformed conformation of H3 HA after triggering by acidic conditions rather than an aggregation of H3.

Das and his colleagues proposed that HA in an acidic environment appeared in several intermediates. However, these intermediate conformations are unknown as smFRET only shows fluorescent signals.[23] Furthermore, the team also found that HA in acidic conditions underwent an irreversible conformational change in the presence of liposomes. We postulated that the Y-shape is the intermediate conformation of H3, and this led us to investigate the interaction between H3 HA and lipid layers in an acidic environment using HS-AFM. Previously, membrane fusion of IAV was demonstrated by mixing either IAV and liposomes[43] or HA−liposome and HA receptor−liposome.[44] These experiment settings are difficult to illustrate clearly regarding the conformational dynamics of HA, while interacting with the lipid layer. Instead of liposomes, we used a native extracellular organelle, the

https://dx.doi.org/10.1021/acs.nanolett.0c01755
Nano Lett. 2020, 20, 6320−6328

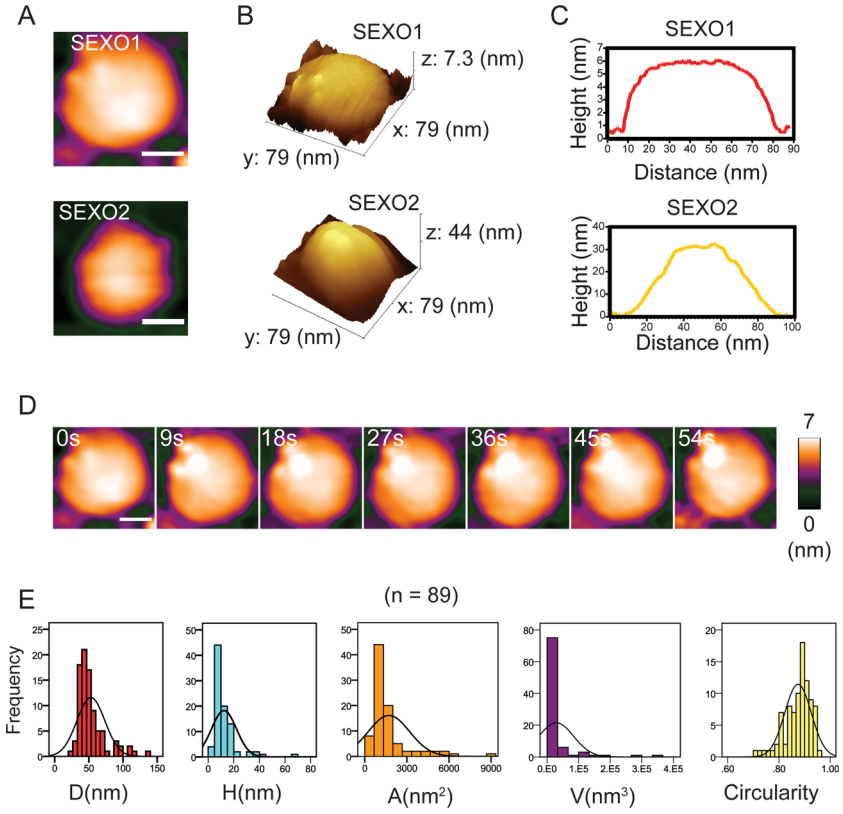

Figure 3. Real-time observation of exosomes in neutral buffer captured by HS-AFM. (A–C) The size of the exosomes isolated from the PC-9 cell line was heterogeneous. (A) HS-AFM images of single exosomes (SEXO) in their native structure (scale bar: 25 nm). (B) 3D structure of SEXO generated using Gwyddion software. (C) Cross-sectional analysis of exosomes, indicating that the height and apical area of exosomes were heterogeneous. (D) Image sequence of real-time imaging of SEXO1. Contact between the cantilever and exosome did not significantly damage the structure of the exosome (scale bar: 25 nm). (E) Spatial dimension analysis of exosomes. Quantitative data were computed from HS-AFM images using ImageJ. Results are presented in histograms with normal distribution curves (D = diameter, H = height, A = area, V = volume).

exosomes, as the source of the target lipid membrane. Exosomes are derived from the intraluminal vesicles (ILVs) of multivesicular bodies (MVBs) or late endosomes.[45] The origin of exosomes suggests that it could be a better option than liposomes for mimicking the endosomal membrane. We managed to isolate high-purity and clean exosomes secreted by PC-9 lung adenocarcinoma cells using Tim-4 affinity purification as reported previously.[46] Before we proceeded, we first studied the nanotopographical features of exosomes using HS-AFM because the information on real-time imaging of exosomes is currently lacking. The exosomes were easily adsorbed onto the bare mica, or the immobilization effect could be enhanced by coating poly-L-lysine (PLL) on mica. We found that the sizes of exosomes were heterogeneous (diameter = 24–133 nm; height = 4–70 nm) as shown in Figure 3A–C (see also, Figure S5A,B,E–G and Movie 5A–D). Real-time scanning demonstrated that exosomes were elastic spherical fluid-filled lipid sacs (Figure 3D and Figure S5E–G). The medium of scanning is important to ensure the native exosome structure can be preserved. In liquid, exosomes exist in their native spherical structure.[47] Spatial dimension analysis of the exosomes was performed, and the results are presented in Figure 3E. Fast Fourier transform (FFT) was conducted to improve the clarity of the images (Figure S5C,D and Movies 5E–H). The lipid texture of the exosomal membrane was smooth, and the center of the exosomes was bulged out as exosomal contents accumulated here. Several studies have reported that the exosomes contain the cytosol of the parental cells, proteins (chemokines/cytokines), nucleic acids, microRNA, RNA, and DNA.[48,49] To further investigate these exosomal materials, we resuspended exosomes in Mili-Q water and then sonicated for 20 min. HS-AFM scanning revealed that some exosomes were deformed. The spherical structure of exosomes remained intact, but the center bulges were shrunken (Figure S6A–C and Movie 6A–C). These results could imply that the deformation of exosome caused leakage of exosomal contents. To rupture exosomes completely, exosomes in Mili-Q water underwent three cycles of freeze–thaw (between room temperature and −80 °C) and then were sonicated for 20 min. We found that exosomes were completely ruptured into remnants (Figure S6D–F and Movie 6D–F). Remarkably, we noticed that there was a filament attached together with the deformed exosome (Figure S7A and Movie 7A). In addition, we also found similar findings after exosomes were ruptured (Figure S7B–E and Movie 7B–E). These filaments can be peptide fragments or nucleic acid filaments.

To record the interaction between HA and exosomes in acidic conditions, we first loaded exosomes on PLL-coated mica and then scanned one particular exosome. After we located the exosome, we paused the scanning and then added H3 HA into the chamber. Scanning was then resumed to record the interaction. We captured the trajectory of a H3 HA that approached and attached to the exosome (Figure 4A and Movie 8). This finding demonstrates that HS-AFM is capable of scanning two objects (H3 HA and exosome) with huge

https://dx.doi.org/10.1021/acs.nanolett.0c01755
Nano Lett. 2020, 20, 6320–6328

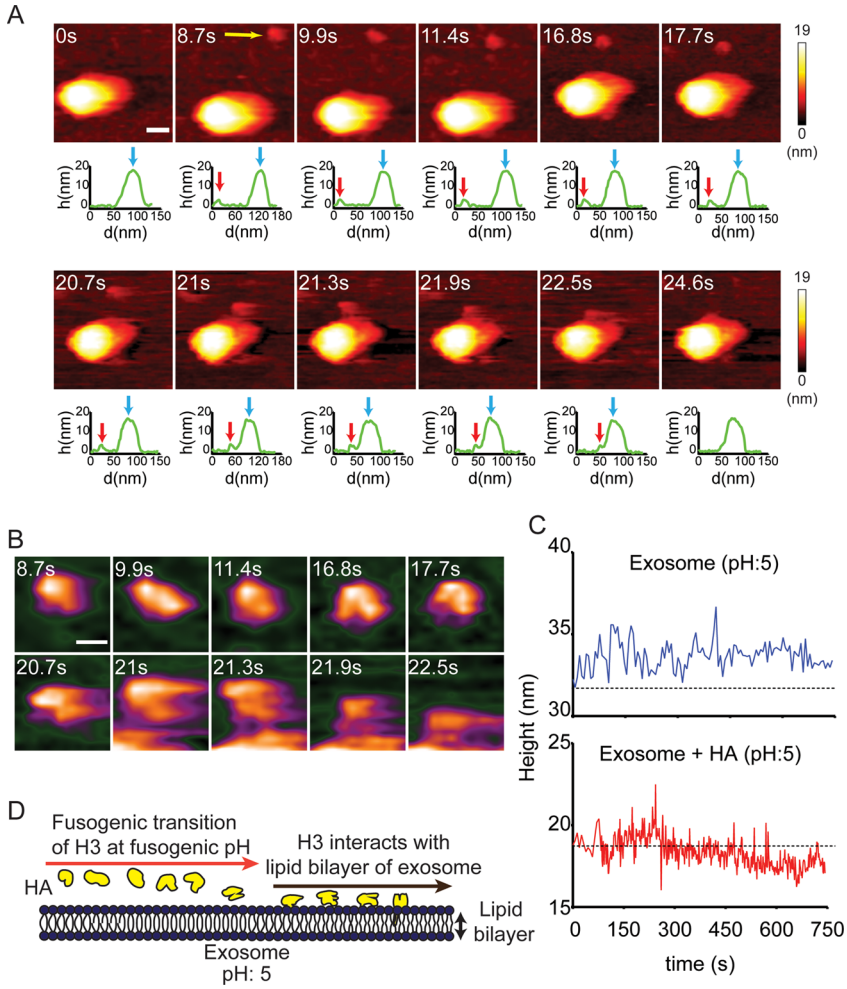

Figure 4. Real-time interaction between the H3 HA and exosome in an acidic buffer recorded using HS-AFM. (A) Interaction between the H3 HA and exosome. Exosomes were immobilized on PLL-coated mica and scanned in an acidic buffer. H3 HA was subsequently added into the chamber. HS-AFM captured a single H3 HA (marked with a yellow arrow) approaching and interacting with an exosome (scale bar: 25 nm). The graphs beneath each frame represent the distance between the H3 HA and the exosome (d = distance; h = height; red arrow = H3 HA; blue arrow = exosome). (B) Image sequence shows the conformational change of the H3 HA when it was interacting with the exosome (scale bar: 10 nm). (C) Real-time measurement of the height of the exosome after it had interacted with the H3 HA. The real-time measurement of the height of an exosome only was used as a control. The lines represent the height of the exosome at $t = 0$ (for control, it refers to the starting time of HS-AFM scanning; for H3 HA-exosome, it refers to the time when H3 HA had contacted to exosome). (D) Schematic diagram illustrating the conformational changes of an H3 HA, while interacting with an exosome in an acidic environment. The exosomal membrane served as a target membrane for the H3 HA to attach to it.

differences in size. While the H3 HA was approaching the exosome, it underwent conformational changes, and the Y-conformation was reproducibly observed again (Figure 4B, Movie 8). Likewise, we also observed that H1 HA attached to an exosome (Figure S8A and Movie 9) in an acidic buffer, and subsequently, it underwent conformational change (Figure S8B and Movie 9). On the basis of these findings, we believe that the Y-shape is the intermediate conformation of HA triggered by the acidic environment. The exosomal lipid bilayer served as a hydrophobic platform for the hydrophobic moiety of the fusion peptide. With this hydrophobic platform, the fusion peptide could be released from its hydrophobic pocket and then inserted into the lipid layer. Previously, Boulay et al. reported that the hydrophobic moiety of the fusion peptide was necessary for HA to bind with the nonionic detergent and liposome.[50] Here, we propose the schematic model of the H3 HA–exosome interaction in Figure 4D.

Insertion of the fusion peptide into the endosomal membrane destabilized the lipid layer and induced membrane fusion.[51] Interestingly, the destabilization of the liposomal lipid bilayer by fusion peptides alone induced rapid expansion of the membrane and subsequent to membrane deformation. These defects could lead to leakage, shrinkage, or membrane rupture of exosomes.[51−54] In our experiment, a declining trend in the height of an exosome after an interaction with H3 HA was found (Figure 4C). In addition, HS-AFM images revealed that the exosomal layer was deformed (Figure S9). We used 1% Triton X-100 to lyse the exosomes and used it as a positive control (Figure S9). We also found that the exosome shrunk after H1 HA had bound to it (Figure S9). The shrunken exosome lost its spherical shape, the center bulge became smaller, and the edge was blebbing. To investigate the outcomes of HA-mediated lipolysis in a low-pH environment, we incubated H3 HA and exosomes in an acidic buffer at room temperature for 30 min prior to HS-AFM scanning. Notably,

https://dx.doi.org/10.1021/acs.nanolett.0c01755
Nano Lett. 2020, 20, 6320−6328

we found membrane remnants (Figure S10 and Movie 10) and peptide fragments or nucleic acid-like filaments (Figure S11 and Movie 11) in these samples. These materials are similar to those found after rupturing exosomes by harsh maneuvers as mentioned earlier (Figures S6 and S7). Therefore, we believe that the fusogenic transformed HA ruptured exosomes, thus releasing exosomal contents.

Previous studies have mentioned that microparticles and exosome-like vesicles in bronchoalveolar lavage fluid neutralized IAV and prevented IAV infection.[55,56] These microparticles and exosome-like vesicles contain $\alpha 2-6$ sialic acid, the receptor of human IAV HA. To observe this phenomenon, we used HS-AFM to visualize the interaction between HA and exosomes in a neutral buffer. The neutral environment was used to mimic the respiratory tract environment. We were able to observe the real-time interaction between HA and exosomes (Figures S12 and 13 and Movies 12 and 13). HA did not undergo conformational changes, and exosomes did not shrink throughout the scanning. We compared the characteristic of the HA−exosome interaction in low-pH and neutral environments and found that the difference was significant (Figure S14 and Movies 14 and 15). The interaction between HA and exosome in an neutral environment was relatively frail as the attachment was weak and reversible. However, the interaction between the HA and exosome in the acidic environment was firm. This observation is reasonable as the HA−exosome interaction in a neutral environment is mediated by RBS and the receptor, which requires weak bonding such as van der Waals bonding and hydrogen bonding.[57] In contrast, the HA−exosome interaction in the acidic environment involves the insertion of the fusion peptide into the exosomal lipid layer.

In summary, by using HS-AFM, we have successfully and directly visualized the native conformation of HA, the fusogenic transition of HA, the native structure of exosomes, and the interaction between the HA and exosome in a real-time fashion. More importantly, these results reflect the molecular behavior of HA during IAV entry, starting from endocytosis to membrane fusion. Our study illustrates the topology of the quaternary structure of HA ectodomains in response to an acidic environment. Since labeling is unnecessary for HS-AFM scanning, we can now observe the inherent molecular dynamic of HA. Furthermore, the nanoscopic spatial resolution and subsecond temporal resolution of HS-AFM are useful for capturing the rapid changing transient conformation of HA during the fusogenic transition. Our data indicate that dissociation of the trimeric globular head domain of HA1 could be the initial step of the fusogenic transition. Interestingly, we did not find any protrusion of the extended coiled-coil structure throughout the HS-AFM recording. This finding suggests that the Y-shape could be a stable HA intermediate and that a fusion peptide may still sequester in the hydrophobic pocket until the target membrane is available. Such interpretation can be explained by two distinct patterns of the HA−exosome interaction, and they are pH-dependent: a firm interaction in an acidic condition but a weak interaction in a neutral condition. In neutral conditions, the trimeric globular head domain of HA1 is conserved, and hence, the HA−exosome interaction could only be mediated by weak bonds such as van der Waals and hydrogen bonds between RBS of HA and receptors in exosomes. In contrast, at a fusogenic pH, protonation of the trimeric globular head domain of HA1 causes its dissociation. In the presence of the exosomal membrane, which serves as a hydrophobic platform, the fusion peptide could release and insert into the exosomal membrane to form a strong interaction, which is reflected as a significantly long interaction time between the HA and exosome in an acidic buffer compared with that in a neutral buffer and destabilization of an exosomal membrane layer, resulting in the deformation or rupture of exosome and leakage of exosomal contents (peptide fragments or nucleic acid-like filaments). Altogether, we propose that the fusogenic transition of HA is likely fit to the "uncaging" model. HS-AFM has opened a new imaging paradigm, in which only a small amount of samples is needed for meaningful scientific observation. Such thought is similar to the difference between nanomedicine and conventional medicine. With a small amount of HA, we can overcome the aggregation issue and focus on single HA molecules to study its conformational dynamic, especially to observe the fusogenic transition.

This study strongly suggests that HS-AFM is a feasible tool, not only for investigating the molecular dynamic of viral fusion proteins but also for visualizing the interaction between viral fusion proteins and their target membranes. In addition, interactions between other viral factors and host factors, for example, an interaction between IAV NS1 and host nucleocytoplasmic trafficking proteins that is needed for passing through a nuclear pore complex (NPC), also can be visualized using HS-AFM in the near future.[58,59]

■ ASSOCIATED CONTENT

Supporting Information

The Supporting Information is available free of charge at https://pubs.acs.org/doi/10.1021/acs.nanolett.0c01755.

Details on experimental methods, (native conformation of H1 and H3 HA, fusogenic transition of H3 HA, nanotopographical features of exosomes, exosome remnants and exosomal contents captured by HS-AFM, interaction between the HA and exosome in acidic conditions, effect of the HA−exosome interaction in an acidic buffer on exosomes, interaction between the HA and exosome in neutral conditions, and difference in the HA−exosome interaction pattern in acidic and neutral conditions), spatial analysis of H3 and H1 measured by Imagej using HS-AFM images or measured by JSmol using PDB data, and movie captions (PDF)

Movie 1 (MP4)
Movie 2 (MP4)
Movie 3 (MP4)
Movie 4 (MP4)
Movie 5 (MP4)
Movie 6 (MP4)
Movie 7 (MP4)
Movie 8 (MP4)
Movie 9 (MP4)
Movie 10 (MP4)
Movie 11 (MP4)
Movie 12 (MP4)
Movie 13 (MP4)
Movie 14 (MP4)
Movie 15 (MP4)

■ AUTHOR INFORMATION

Corresponding Author

Richard W. Wong − *WPI-Nano Life Science Institute and Cell-Bionomics Research Unit, Institute for Frontier Science Initiative*

https://dx.doi.org/10.1021/acs.nanolett.0c01755
Nano Lett. 2020, 20, 6320−6328

(INFINITI), Kanazawa University, Kanazawa, Ishikawa, Japan; orcid.org/0000-0002-2131-6595; Phone: 81-76-264-6250; Email: rwong@staff.kanazawa-u.ac.jp; Fax: 81-76-264-6253

Authors

Keesiang Lim – *WPI-Nano Life Science Institute, Kanazawa University, Kanazawa, Ishikawa, Japan*

Noriyuki Kodera – *WPI-Nano Life Science Institute, Kanazawa University, Kanazawa, Ishikawa, Japan*

Hanbo Wang – *Cell-Bionomics Research Unit, Institute for Frontier Science Initiative (INFINITI), Kanazawa University, Kanazawa, Ishikawa 920-1192, Japan*

Mahmoud Shaaban Mohamed – *Cell-Bionomics Research Unit, Institute for Frontier Science Initiative (INFINITI), Kanazawa University, Kanazawa, Ishikawa 920-1192, Japan*

Masaharu Hazawa – *WPI-Nano Life Science Institute and Cell-Bionomics Research Unit, Institute for Frontier Science Initiative (INFINITI), Kanazawa University, Kanazawa, Ishikawa, Japan*

Akiko Kobayashi – *Cell-Bionomics Research Unit, Institute for Frontier Science Initiative (INFINITI), Kanazawa University, Kanazawa, Ishikawa 920-1192, Japan*

Takeshi Yoshida – *WPI-Nano Life Science Institute, Kanazawa University, Kanazawa, Ishikawa, Japan; Department of Immunology, Kanazawa University Graduate School of Medical Sciences, Kanazawa, Ishikawa 920-8640, Japan*

Rikinari Hanayama – *WPI-Nano Life Science Institute, Kanazawa University, Kanazawa, Ishikawa, Japan; Department of Immunology, Kanazawa University Graduate School of Medical Sciences, Kanazawa, Ishikawa 920-8640, Japan*

Seiji Yano – *WPI-Nano Life Science Institute and Division of Medical Oncology, Cancer Research Institute, Kanazawa University, Kanazawa, Ishikawa, Japan*

Toshio Ando – *WPI-Nano Life Science Institute, Kanazawa University, Kanazawa, Ishikawa, Japan;* orcid.org/0000-0001-8819-154X

Complete contact information is available at: https://pubs.acs.org/10.1021/acs.nanolett.0c01755

Author Contributions

K.L. and R.W. designed the study and wrote the manuscript. K.L. performed the experiments and prepared figures. N.K. performed AFM simulation, and H.W., M.S.M., K.M., M.H., S.Y., A.K., and T.A. analyzed the data. T.Y. and R.H. prepared exosomes. All authors read and approved the final manuscript. R.W. supervised the whole study.

Funding

This project was funded by grants from the MEXT/JSPS KAKENHI (19K23841, 20K16262 (to K.L.), 17H05874, 17K08655 (to R.W.)) from MEXT Japan, from the Kobayashi International Scholarship Foundation (to R.W.), and the Shimadzu Science Foundation (to R.W.).

Notes

The authors declare no competing financial interest.

■ ACKNOWLEDGMENTS

We thank the members of the Ando, Yano, Kodera, and Hanayama laboratories for their critical feedback and discussion.

■ REFERENCES

(1) Krammer, F.; Smith, G. J. D.; Fouchier, R. A. M.; Peiris, M.; Kedzierska, K.; Doherty, P. C.; Palese, P.; Shaw, M. L.; Treanor, J.; Webster, R. G.; Garcia-Sastre, A. Influenza. *Nat. Rev. Dis Primers* **2018**, *4* (1), 3.

(2) Lozano, R.; et al. Global and regional mortality from 235 causes of death for 20 age groups in 1990 and 2010: a systematic analysis for the Global Burden of Disease Study 2010. *Lancet* **2012**, *380* (9859), 2095–128.

(3) Mair, C. M.; et al. Receptor binding and pH stability - how influenza A virus hemagglutinin affects host-specific virus infection. *Biochim. Biophys. Acta, Biomembr.* **2014**, *1838* (4), 1153–68.

(4) Wiley, D. C.; Skehel, J. J. The structure and function of the hemagglutinin membrane glycoprotein of influenza virus. *Annu. Rev. Biochem.* **1987**, *56*, 365–94.

(5) Carr, C. M.; Kim, P. S. A spring-loaded mechanism for the conformational change of influenza hemagglutinin. *Cell* **1993**, *73* (4), 823–32.

(6) Skehel, J. J.; Wiley, D. C. Receptor binding and membrane fusion in virus entry: the influenza hemagglutinin. *Annu. Rev. Biochem.* **2000**, *69*, 531–69.

(7) Wharton, S. A.; et al. Electron microscopy of antibody complexes of influenza virus haemagglutinin in the fusion pH conformation. *EMBO J.* **1995**, *14* (2), 240–6.

(8) Zhang, Y.; et al. Targeting Hemagglutinin: Approaches for Broad Protection against the Influenza A Virus. *Viruses* **2019**, *11* (5), 405.

(9) Bullough, P. A.; et al. Structure of influenza haemagglutinin at the pH of membrane fusion. *Nature* **1994**, *371* (6492), 37–43.

(10) Garcia, N. K.; et al. Dynamic changes during acid-induced activation of influenza hemagglutinin. *Structure* **2015**, *23* (4), 665–76.

(11) Chen, J.; Skehel, J. J.; Wiley, D. C. N- and C-terminal residues combine in the fusion-pH influenza hemagglutinin HA(2) subunit to form an N cap that terminates the triple-stranded coiled coil. *Proc. Natl. Acad. Sci. U. S. A.* **1999**, *96* (16), 8967–72.

(12) Bizebard, T.; et al. Structure of influenza virus haemagglutinin complexed with a neutralizing antibody. *Nature* **1995**, *376* (6535), 92–4.

(13) Krumbiegel, M.; Herrmann, A.; Blumenthal, R. Kinetics of the low pH-induced conformational changes and fusogenic activity of influenza hemagglutinin. *Biophys. J.* **1994**, *67* (6), 2355–60.

(14) Remeta, D. P.; et al. Acid-induced changes in thermal stability and fusion activity of influenza hemagglutinin. *Biochemistry* **2002**, *41* (6), 2044–54.

(15) Han, X.; et al. Membrane structure and fusion-triggering conformational change of the fusion domain from influenza hemagglutinin. *Nat. Struct. Biol.* **2001**, *8* (8), 715–20.

(16) Lorieau, J. L.; et al. pH-triggered, activated-state conformations of the influenza hemagglutinin fusion peptide revealed by NMR. *Proc. Natl. Acad. Sci. U. S. A.* **2012**, *109* (49), 19994–9.

(17) Doms, R. W.; Helenius, A.; White, J. Membrane fusion activity of the influenza virus hemagglutinin. The low pH-induced conformational change. *J. Biol. Chem.* **1985**, *260* (5), 2973–81.

(18) Kemble, G. W.; et al. Intermonomer disulfide bonds impair the fusion activity of influenza virus hemagglutinin. *J. Virol.* **1992**, *66* (8), 4940–50.

(19) Skehel, J. J.; et al. Changes in the conformation of influenza virus hemagglutinin at the pH optimum of virus-mediated membrane fusion. *Proc. Natl. Acad. Sci. U. S. A.* **1982**, *79* (4), 968–72.

(20) White, J. M.; Wilson, I. A. Anti-peptide antibodies detect steps in a protein conformational change: low-pH activation of the influenza virus hemagglutinin. *J. Cell Biol.* **1987**, *105* (6), 2887–2896.

(21) Fontana, J.; et al. Structural changes in Influenza virus at low pH characterized by cryo-electron tomography. *J. Virol* **2012**, *86* (6), 2919–29.

(22) Bottcher, C.; et al. Structure of influenza haemagglutinin at neutral and at fusogenic pH by electron cryo-microscopy. *FEBS Lett.* **1999**, *463* (3), 255–9.

(23) Das, D. K.; et al. Direct Visualization of the Conformational Dynamics of Single Influenza Hemagglutinin Trimers. *Cell* **2018**, *174* (4), 926−937.
(24) Godley, L.; et al. Introduction of intersubunit disulfide bonds in the membrane-distal region of the influenza hemagglutinin abolishes membrane fusion activity. *Cell* **1992**, *68*, 635−645.
(25) Kemble, G. W.; et al. Intermonomer disulfide bonds impair the fusion activity of influenza virus hemagglutinin. *J. Virol.* **1992**, *66* (8), 4940−4950.
(26) Leikina, E.; et al. Reversible stages of the low-pH-triggered conformational change in influenza virus hemagglutinin. *EMBO J.* **2002**, *21* (21), 5701−10.
(27) Stegmann, T.; et al. The HA2 subunit of influenza hemagglutinin inserts into the target membrane prior to fusion. *J. Biol. Chem.* **1991**, *266* (27), 18404−10.
(28) Harrison, S. C. Viral membrane fusion. *Nat. Struct. Mol. Biol.* **2008**, *15* (7), 690−8.
(29) Huang, Q.; et al. Early steps of the conformational change of influenza virus hemagglutinin to a fusion active state: stability and energetics of the hemagglutinin. *Biochim. Biophys. Acta, Biomembr.* **2003**, *1614* (1), 3−13.
(30) Ando, T. High-speed atomic force microscopy. *Curr. Opin. Chem. Biol.* **2019**, *51*, 105−112.
(31) Ando, T.; Uchihashi, T.; Kodera, N. High-speed AFM and applications to biomolecular systems. *Annu. Rev. Biophys.* **2013**, *42*, 393−414.
(32) Uchihashi, T.; et al. High-speed atomic force microscopy reveals rotary catalysis of rotorless F(1)-ATPase. *Science* **2011**, *333* (6043), 755−8.
(33) Kodera, N.; et al. Video imaging of walking myosin V by high-speed atomic force microscopy. *Nature* **2010**, *468* (7320), 72−6.
(34) Mohamed, M. S.; et al. Spatiotemporally tracking of nano-biofilaments inside the nuclear pore complex core. *Biomaterials* **2020**, *256*, 120198.
(35) Mohamed, M. S.; et al. High-Speed Atomic Force Microscopy Reveals Loss of Nuclear Pore Resilience as a Dying Code in Colorectal Cancer Cells. *ACS Nano* **2017**, *11* (6), 5567−5578.
(36) Lim, K. S.; et al. Direct visualization of avian influenza H5N1 hemagglutinin precursor and its conformational change by high-speed atomic force microscopy. *Biochim. Biophys. Acta, Gen. Subj.* **2020**, *1864* (2), 129313.
(37) Doms, R. W.; Helenius, A. Quaternary structure of influenza virus hemagglutinin after acid treatment. *J. Virol.* **1986**, *60* (3), 833−9.
(38) Wilson, I. A.; Skehel, J. J.; Wiley, D. C. Structure of the haemagglutinin membrane glycoprotein of influenza virus at 3 A resolution. *Nature* **1981**, *289* (5796), 366−73.
(39) Ando, T. High-speed atomic force microscopy and its future prospects. *Biophys. Rev.* **2018**, *10* (2), 285−292.
(40) Bullough, P. A.; et al. Crystals of a fragment of influenza haemagglutinin in the low pH induced conformation. *J. Mol. Biol.* **1994**, *236* (4), 1262−5.
(41) Ruigrok, R. W. H.; Aitken, A.; Calder, L. J.; Martin, S. R.; Skehel, J. J.; Wharton, S. A.; Weis, W.; Wiley, D. C. Studies on the structure of the influenza virus haemagglutinin at the pH of membrane fusion. *J. Gen. Virol.* **1988**, *69* (11), 2785−2795.
(42) Ruigrok, R. W.; et al. Electron microscopy of the low pH structure of influenza virus hemagglutinin. *EMBO J.* **1986**, *5* (1), 41−49.
(43) Calder, L. J.; Rosenthal, P. B. Cryomicroscopy provides structural snapshots of influenza virus membrane fusion. *Nat. Struct. Mol. Biol.* **2016**, *23* (9), 853−8.
(44) Lee, H.; Jin, W.; Jeong, B.-C.; Suh, J.-W. A new in vitro hemagglutinin inhibitor screening system based on a single-vesicle fusion assay. *Sci. Rep.* **2016**, *6*, 30642.
(45) Skotland, T.; et al. Exosomal lipid composition and the role of ether lipids and phosphoinositides in exosome biology. *J. Lipid Res.* **2019**, *60* (1), 9−18.
(46) Nakai, W.; Yoshida, T.; Diez, D.; Miyatake, Y.; Nishibu, T.; Imawaka, N.; Naruse, K.; Sadamura, Y.; Hanayama, R. A novel affinity-based method for the isolation of highly purified extracellular vesicles. *Sci. Rep.* **2016**, *6*, 33935.
(47) Parisse, P.; et al. Atomic force microscopy analysis of extracellular vesicles. *Eur. Biophys. J.* **2017**, *46* (8), 813−820.
(48) Valadi, H.; et al. Exosome-mediated transfer of mRNAs and microRNAs is a novel mechanism of genetic exchange between cells. *Nat. Cell Biol.* **2007**, *9* (6), 654−9.
(49) Kahlert, C.; et al. Identification of double-stranded genomic DNA spanning all chromosomes with mutated KRAS and p53 DNA in the serum exosomes of patients with pancreatic cancer. *J. Biol. Chem.* **2014**, *289* (7), 3869−75.
(50) Boulay, F.; et al. The influenza hemagglutinin precursor as an acid-sensitive probe of the biosynthetic pathway. *EMBO J.* **1987**, *6* (9), 2643−50.
(51) Longo, M. L.; Waring, A. J.; Hammer, D. A. Interaction of the influenza hemagglutinin fusion peptide with lipid bilayers: area expansion and permeation. *Biophys. J.* **1997**, *73* (3), 1430−9.
(52) Sato, S. B.; Kawasaki, K.; Ohnishi, S. Hemolytic activity of influenza virus hemagglutinin glycoproteins activated in mildly acidic environments. *Proc. Natl. Acad. Sci. U. S. A.* **1983**, *80* (11), 3153−7.
(53) Jiricek, R.; Schwarz, G.; Stegmann, T. Pores formed by influenza hemagglutinin. *Biochim. Biophys. Acta, Biomembr.* **1997**, *1330* (1), 17−28.
(54) Nomura, F.; et al. Microscopic observations reveal that fusogenic peptides induce liposome shrinkage prior to membrane fusion. *Proc. Natl. Acad. Sci. U. S. A.* **2004**, *101* (10), 3420−5.
(55) Kesimer, M.; et al. Characterization of exosome-like vesicles released from human tracheobronchial ciliated epithelium: a possible role in innate defense. *FASEB J.* **2009**, *23* (6), 1858−68.
(56) Suptawiwat, O.; et al. Microparticle and anti-influenza activity in human respiratory secretion. *PLoS One* **2017**, *12* (8), No. e0183717.
(57) Haywood, A. M.; Boyer, B. P. Fusion of influenza virus membranes with liposomes at pH 7.5. *Proc. Natl. Acad. Sci. U. S. A.* **1985**, *82* (14), 4611−5.
(58) Zhang, K.; et al. Structural basis for influenza virus NS1 protein block of mRNA nuclear export. *Nat. Microbiol* **2019**, *4* (10), 1671−1679.
(59) Wong, R. W.; Mamede, J. I.; Hope, T. J. Impact of Nucleoporin-Mediated Chromatin Localization and Nuclear Architecture on HIV Integration Site Selection. *J. Virol.* **2015**, *89* (19), 9702−5.

https://dx.doi.org/10.1021/acs.nanolett.0c01755
Nano Lett. 2020, 20, 6320−6328